Characterizing archaeological bronze corrosion products intersecting electrochemical impedance measurements with voltammetry of immobilized particles

Jorge Redondo-Marugán[a], Joan Piquero-Cilla[b], María Teresa Doménech-Carbó[a], Blanca Ramírez-Barat[c], Wassef Al Sekhaneh[d], Sofia Capelo*[e], Antonio Doménech-Carbó*[b]

[a] Institut de Restauració del Patrimoni, Universitat Politècnica de València, Camí de Vera 14, 46022, València, Spain.
[b] Departament de Química Analítica. Universitat de València. Dr. Moliner, 50, 46100 Burjassot (València) Spain.
[c] Centro Nacional de Investigaciones Metalúrgicas (CENIM), Consejo Superior de Investigaciones Científicas (CSIC), Avda. Gregorio del Amo 8, 28040 Madrid.
[d] Faculty of Anthropology and Archaeology,Yarmouk University Irbid-Jordan.
[e] Centro Interdisciplinar de História, Culturas e Sociedades da Universidade de Évora (CIDEHUS/UE) & Departamento de Paisagem, Ambiente e Ordenamento, Escola de Ciências e Tecnologia, Universidade de Évora, Rua Romão Ramalho 59, 7000-671 Évora Portugal.

* Corresponding authors, e-mail: scapelo@uevora.pt, antonio.domenech@uv.es

Abstract

Application of electrochemical impedance measurements to microparticulate deposits of copper corrosion products attached to graphite electrodes in contact with 0.10 M aqueous $HClO_4$ electrolyte is described. The impedance measurements were sensitive to the applied potential and the amount of solid sample and were modeled taking into account the contribution of the uncovered base electrode. Several pairs of circuit elements provide monotonic variations which are able to characterize different corrosion compounds regardless the amount of microparticulate solid on the electrode. Application to a set of archaeological samples from the archaeological Roman site of Gadara (Jordan, 4th century AD) permitted to establish a grouping of such samples suggesting different provenances/manufacturing techniques.

Keywords: Archaeological bronze; Electrochemical Impedance Measurements; Voltammetry of immobilized particles.

1. Introduction

Tracing the provenance and technique of fabrication of archaeological objects are obvious targets for archaeologists, conservators and restorers. In the case of metal artifacts, this information can be derived from the chemical composition of the alloy, isotope ratios, and the microstructure of the alloy and patina from metallographic cross sections [1-4]. In general, however, sampling the metal core is not allowed or seriously restricted for archaeological objects, so that the characterization of the metallic material, manufacturing technique, etc. have to be obtained from the physico-chemical properties of the metal patina [5-8]. For this purpose a wide variety of microscopy, spectroscopy, diffraction and electrochemistry derived techniques have been used [9-15].

In this context, the voltammetry of immobilized particles (VIMP), a solid-state electrochemical methodology developed by Scholz et al. [16,17], was applied to obtain analytical information on archaeological materials [18-20]. This technique, which provides information on sparingly soluble solids attached to inert electrodes, has been applied for identifying [21-25] and quantifying [26] metals and alloys. Sampling strategies based on 'graphite pencil' electrodes [27-29], have been exploited for mapping [30] and layer-by-layer [31] analysis and implemented for characterizing corrosion products [32], authentication [33,34] and dating [35,36].

In turn, electrochemical impedance spectroscopy (EIS), is an electrochemical technique extensively used in the study of metal corrosion [37,38], which has also been applied to characterize archaeological copper/bronze [12,39-43], and dating purposes [44,45]. All these approaches involve the study of the archaeological object or a representative fragment and its placement in contact with a suitable electrolyte, and require the existence of metal core available for establishing electrical contact. In most cases of archaeological interest, however, there is no possibility of accessing to the metallic core and only the more or less consolidated layers of corrosion products are usable for electroanalytical measurements.

Although in these circumstances the VIMP methodology is applicable for identifying corrosion products, even when several electroactive compounds coexist [29,32,45], in

most cases, the archaeological objective is not the exhaustive characterization of the composition of the corrosion layers, but the grouping of the samples for establishing provenances and workshops. Aimed to complement the existing techniques devoted to such analytical purposes, we present here an intersection between EIS and VIMP methodologies specifically directed to its utilization in the archaeological field. For this purpose, impedance measurements of microparticulate deposits of minerals and samples attached to graphite electrodes in contact with different aqueous electrolytes were performed. As an antecedent for this kind of study, that of Retter et al. on the impedance of inhomogeneous composites of hexacyanometallates in contact with aqueous electrolytes [46].

The reported methodology has two main problems: i) the influence of the amount of sample and coverage of the base graphite electrode, and ii) the difficulty of modeling a system where the base graphite electrode is partially covered by a powdered material. Additionally, it should be noted that, strictly, impedance spectroscopy is only defined for a stationary system accomplishing the demands of the linear systems theory (LST) [47,48]. Accordingly, to be considered as 'spectroscopy', the measured system should be time-invariant during the acquisition of the impedance data satisfying the Kramers-Kronig (K-K) transfer functions [49,50]. Since impedance measurements were performed here in conditions promoting to some extent the transient reduction of copper corrosion products, steady state conditions were, although essentially operating (*vide infra*), not strictly attained.

Such problems will be treated in relation to the application of the proposed methodology for screening samples from bronze artifacts from the Roman archaeological site Gadara (Jordan), dated back in the 4th century AD. Complementary VIMP and atomic force microscopy (AFM-VIMP) experiments were performed upon attachment of cuprite microparticulate deposits on graphite plates in contact with aqueous electrolytes.

2. Experimental

2.1. Materials and samples

Reference materials were cuprite (Cu_2O, Merck), tenorite (CuO, Merck), malachite (supplied by Kremer pigments). Brochantite and atacamite reference minerals were supplied by Minerales de Colección, Almuñécar, Spain and Minerales de Torres, Villaviciosa de Odón, Spain. The studied materials, simply referred as samples hereafter, consisted of ca. 500 mg of powders from the corrosion layers of different archaeological objects: 18 fragments of sculptures (samples S1 to S18) and two different sets of cylinders used as balance weights (W1-W3 and P1-P11), all extracted from the Roman archaeological site of Gadara (Jordan), 4^{th} century AD. All objects were made of bronze, often leaded, as determined from VIMP measurements (*vide infra*). Due to the intrinsic archaeological value of the objects, no usual invasive techniques were used for determining the composition of the metallic core. By reasons of patrimony conservation, only the powdered materials from archaeological objects were accessible for electrochemical measurements.

For electrode conditioning, amounts between 0.1 and 1 mg of samples or reference materials were extended on an agate mortar forming a spot of finely distributed material. Then, the graphite electrode was pressed over this layer being further transferred into the electrochemical cell so that only the lower end of the electrode was in contact with the electrolyte. This method of electrode conditioning does not permit to control the amount of deposited particles. The amount of the deposit was approximated by weighting the electrode before and after conditioning. Then, more or less massive deposits were discriminated but, since in the conditioning process a certain amount of graphite was removed, no attempts were made to estimate the weight of deposited particles.

2.2. Electrochemical instrumentation and procedures

VIMP and EIS experiments were performed at sample-modified paraffin-impregnated graphite electrodes using commercial graphite bars (Staedtler Mars 200 HB, geometrical surface area 0.031 cm^2). Different electrolytes of known VIMP response of copper corrosion products [39-43] were tested in order to determine the optimal conditions of repeatability and stability of impedance measurements. Air-saturated 0.10 M $HClO_4$ aqueous solutions at pH 1.0 was selected as the electrolyte. No degasification was carried out in order to test the possibility of using the electrochemical reduction of dissolved

oxygen as a redox probe. All electrochemical measurements were carried out *via* a potentiostat/galvanostat Autolab PGSTAT12 equipped with a Frequency Response Analyzer (FRA2) from Metrohm Autolab B.V. and also a CH I660 potentiostat. A standard three-electrode arrangement was used with a platinum auxiliary electrode and a Ag/AgCl (3M NaCl) reference electrode. VIMP experiments were performed using the aforementioned electrode conditioning and equipment. Square wave voltammetry was used as a detection mode with potential step increment of 4 mV, square wave amplitude of 25 mV (peak-to-peak) and frequency of 5 Hz.

Electrochemical impedance measurements were performed, using the aforementioned instrument, in the 0.01 to 100000 Hz frequency range with an ac sinusoidal perturbation amplitude of 10 mV (peak-to-peak) at different potentials between +1.00 and –1.00 V vs. Ag/AgCl upon immersion of the sample-modified graphite electrode into the electrolyte. Repeatability tests were performed for each one of the samples by performing independently EIS experiments in three freshly prepared sample-modified graphite electrodes. Prior to each EIS experiment, an equilibration time of 5 min was taken.

In situ AFM-monitored electrochemical experiments were run with a multimode AFM (Digital Instruments VEECO Methodology Group, USA) with a NanoScope IIIa controller equipped with a J-type scanner (max. scan size of 150×150×6 μm). The topography of samples was studied in the contact mode. An oxide-sharpened silicon nitride probe Olympus (VEECO Methodology Group, model NP-S) with a V-shaped cantilever configuration was used. The transfer of sample particles to a carbon plate and the experimental conditions were similar to those previously described for studying pictorial pigments [51].

3. Results and discussion

3.1. Voltammetric pattern

The voltammetric response of the more frequent copper corrosion products, atacamite, brochantite, cuprite and malachite has been widely studied [22-26,32,36] consisting, in contact with 0.10 M $HClO_4$, of a main cathodic process at ca. –0.10 V vs. Ag/AgCl, corresponding to the reduction to Cu metal, in all these cases whereas tenorite was

reduced at potentials ca. –0.4 V vs. Ag/AgCl [32,36]. A typical voltammogram of cuprite-modified graphite electrode accompanying the current/time curve obtained for a cuprite deposit when a constant potential of –0.25 V vs. Ag/AgCl was applied is presented as Supplementary information (Figure S.1).

It is pertinent to note that, under our common experimental conditions for VIMP and EIS experiments, the graphite electrode was covered by a discontinuous layer of grains of the corresponding solid compound or archaeological sample. AFM monitoring of cuprite reduction is illustrated in Figure 1 where the topographic images of an aggregate of cuprite crystals a) before and b) after application of a constant potential of –0.25 V vs. Ag/AgCl are shown. Comparison of both images reveals the appearance of some minor topographic features, representative of the formation of crystals of metallic Cu, in the boundary region between the cuprite, the base graphite plate and the electrolyte. These features are consistent with those reported by Hasse and Scholz for in situ AFM monitoring of the reduction process of lead oxide [52] and the description of VIMP experiments on ion –insertion solids [53]. These authors described this process in terms of the topotactic conversion of lead oxide into lead metal. According to this description the cathodic reaction proceeds via the formation of an ionomeric layer between the parent metal oxide and the metal which advances progressively [52]. This layer would be composed by more or less hydrated ions released from the solid particle and entered from the electrolyte. Consistently with this description, small morphological changes observed in Figure 1 are confined to a narrow region in the particle/base electrode/electrolyte three phase boundary and, upon application of a constant potential step, the current decreases rapidly, as shown in Figure S.1. For our purposes, the relevant point to emphasize is that, under the conditions in Figure S.1, an almost stationary response appeared at times longer than 20-25 s and that this response was essentially independent on the amount of copper compound deposited onto the electrode, a feature that will be further treated in relation to the interpretation of EIS data.

3.2. Impedance measurements

The impedance measurements were sensitive to the applied potential, electrolyte and the amount of microparticulate solid attached to the graphite electrode. Keeping in mind the

possibility of discriminating between different copper corrosion products, the differences between the impedance measurements in the presence and in the absence of mineral modifier were investigated in various electrolytes upon varying the bias potential. Based on the ability for discriminating between different copper minerals (vide infra), the selected electrolyte was aqueous 0.10 M $HClO_4$ at pH 1.0. Here, applying bias potentials between +0.25 and –0.75 V vs. Ag/AgCl, the Nyquist plots of the spectra of the tested cooper corrosion products (cuprite, malachite, atacamite, brochantite, tenorite) consisted of a main depressed capacitive loop whose size differed significantly between the bare electrode and the graphite electrode modified with copper compounds depending on the applied bias potential. The spectra presented significant scattering at frequencies below 0.10 Hz; for this reason, although were acquired at frequencies between 10^5 and 0.01 Hz, only data between 10^5 and 0.10 Hz will be presented in the following.

Figure 2a depicts the Nyquist plots for an unmodified graphite electrode and three successive impedance runs on the same cuprite-modified graphite electrode when a bias potential of –0.25 V vs. Ag/AgCl was applied. In all cases, a main depressed capacitive loop was recorded, but the size clearly decreases from the bare graphite electrode to that covered by a fine deposit of cuprite, successive measurements on the same deposit producing a small decrease of the loop size. Figure 2b compares the 1st EIS measurement on freshly prepared cuprite-modified graphite electrodes containing different Cu_2O loadings. Although there is no possibility of an accurate measurement of the amount of cuprite transferred to the electrode, our data indicated that the diameter of the capacitive loop decreased on increasing the amount of this compound.

Figure 3a compares the variation of the logarithm of the impedance modulus ($\log|Z|$) and the (minus) phase angle (φ) on the logarithm of the frequency ($\log f$) in impedance measurements on an unmodified graphite electrode and three successive impedance runs on the same cuprite-modified graphite electrode. The impedance modulus decreased clearly at middle and low frequencies from the graphite electrode to the cuprite-modified electrode while the phase angle displayed a maximum at intermediate frequencies which varied slightly between the different spectra. The corresponding plots for graphite electrodes containing different amounts of cuprite are depicted in Figure 3b.

On increasing the amount of cuprite the total impedance experienced a small decrease at all frequencies whereas the maximum of phase angle diminished slightly.

The impedance at the lower operative frequency, Z_{low}, one of the parameters used by Mallouk et al. to describe the EIS of porous oxides with discrete particles discriminating different compositions [54], was taken at 0.10 Hz in order to illustrate the differences between the EIS data under different experimental conditions. Figure 4a compares the variation of $|Z_{low}|$ on the bias potential, E_{bias}, for an unmodified graphite electrode and electrodes modified with cuprite and malachite (similar results were obtained for brochantite, atacamite and tenorite). The maximum (absolute) value of the phase angle (φ_{max}) at the intermediate frequencies was used as another representative quantity for testing differences between the different corrosion products. Figure 4b compares the variation of $-\varphi_{max}$ on E_{bias} for cuprite-modified electrodes in contact with air-saturated 0.10 M $HClO_4$ aqueous solutions. Although φ_{max} is quite sensitive to changes in the electrolyte resistance, in turn depending on the position of the reference electrode [55], data in Figure 4 were obtained upon maintaining invariable those parameters and varying exclusively the bias potential. Such results indicated that significant differences between the bare electrode and the different graphite-modified electrodes (atacamite, brochantite, cuprite, malachite and tenorite) appeared at bias potentials between +0.4 and –0.4 V vs. Ag/AgCl.

To rationalize the above EIS data it is pertinent to note that the systems under study consisted of a set of microparticles of semiconducting (Cu_2O and CuO) and insulating (calcite, silicates) materials deposited onto a conducting graphite surface where a significant fraction of the graphite surface was directly exposed to the electrolyte. First of all, data in Figure 4 indicate that the EIS response was notably influenced by the occurrence of Faradaic processes. Applying bias potentials between +0.4 and 0.0 V vs. Ag/AgCl (region I in Figure 4a), no Faradaic processes occur and the spectra of the unmodified graphite electrode was similar to that of electrodes modified with reference copper compounds, all displaying high impedance (Z_{low}) values. In the region of bias potentials around –0.25 V vs. Ag/AgCl (region II in Figure 4a), where the reduction of such copper compounds takes place, the impedance of the unmodified graphite becomes clearly larger than those of the different compound-modified electrodes. Remarkably, in

this region, there are also differences between both the Z_{low} and φ_{max} values of the different copper compounds (see Figures 4a and 4b). Finally, at potentials below –0.40 V vs. Ag/AgCl (region III in Figure 4a), in which proton discharge starts to occur in the used electrolyte, the EIS parameters become again similar for modified and unmodified electrodes. This feature suggests that in these conditions, the EIS response is dominated by charge transfer via hydrogen evolution reaction (HER) at the bare graphite. In order to promote the major sensitivity of the EIS response to the nature of the electrode modifier, experiments were conducted upon application of a bias potential of –0.25 V vs. Ag/AgCl.

To interpret the apparent contradiction between the impedance decrease in successive measurements on the same modified electrode (Figs. 2a, 3a,c) and the impedance decrease on 'first scan' spectra on increasing the amount of cuprite (Figs. 2b, 3b,d), it is pertinent to consider the peculiar nature of the modified electrodes used in VIMP-EIS experiments, consisting of a conducting graphite surface partially covered by a microparticulate deposit of semiconducting and/or insulating materials. In EIS experiments, the propagation of the sinusoidal signal (roughly, charge transfer phenomena) can theoretically occur through a) The bare graphite and the electrolyte (route (i) depicted in the scheme provided as a Figure S.2 in Supplementary materials); b) the graphite/crystal and the crystal electrolyte interfaces via electron/hole transport through the crystal (route (ii) in Figure S.2) by means of the occurrence of Faradaic processes. In the case of the reduction of copper compounds, according to the descriptions in VIMP literature [16,17], the Faradaic process initiates through the solid particle/base electrode/electrolyte three-phase junction [55] via the simultaneous transfer of protons from the electrolyte to the solid particle and electrons from the base electrode to the solid particle giving rise to the presumably topotactic formation of copper crystals in the immediate vicinity of the crystals of the parent copper compound being separated by an ionomeric, highly hydrated layer as described for the electrochemical reduction of lead compounds [52] (route (iv) in Figure S.2).

Under the application of a bias potential of –0.25 V vs. Ag/AgCl (region II in Figure 4a), the Faradaic process of the reduction of cuprite, atacamite, malachite, etc. dominated the EIS response and determined a decrease of the impedance relative to that

of the unmodified electrode, this effect being increased upon attaching increasing amounts of copper compound to the graphite surface as depicted in Figures 2b, 3b. On the other hand, the growth of the metal deposit adjacent to the grains of parent copper compound provides opportunity of a Faradaic charge transfer route via the metal/ionomeric layer and ionomeric layer/copper compound interfaces (route (iv) in Figure S.2). Accordingly, the slight decrease of the charge transfer impedance observed in successive EIS runs on the same modified electrode (Figures 2a and 3a) can be interpreted in terms of the increasing occurrence of charge transport via this route.

The conditions of operation were selected from a compromise between repeatability and sensitivity (in terms of the differences such as depicted in Figure 4); 0.10 M $HClO_4$ at pH 1.0 and bias potential of –0.25 V vs. Ag/AgCl were adopted. Under the application of this potential, the reduction of copper corrosion products of the malachite (copper hydroxycarbonates), brochantite (copper hydroxysulfates) and atacamite (copper hydroxychlorides) should occur [21-26,31] so that, strictly, the system operates under non-steady state conditions. In these circumstances, the performed electrochemical impedance measurements cannot be strictly considered as impedance spectra [47-50]. In the conditions used here, coincident with those used in VIMP studies of copper corrosion products [21-26], the progress of the reaction is slow enough so that, as suggested by data in Figures 1 and S.1 and in coincidence with EIS studies on metal corrosion using acidic electrolytes [56] and different bias potentials [57], one can assume that steady-state conditions of operation are attained.

Interestingly, different pairs of impedance quantities experienced monotonical variations with the amount of mineral which were characteristic of the different copper corrosion products. This can be seen in Figure 5 where the variation of $-Z_{imag}$ vs. Z_{real} measured at the extreme low frequency (0.1 Hz) is plotted for microparticulate deposits of cuprite, malachite, brochantite and atacamite. Noticeably, the data points for the successive impedance runs on each modified electrode (the situation depicted in Figures 2a, 3a,c) fall in the same curved line lying with the data points for the 1^{st} run on the deposits with different mineral loadings (the situation depicted in Figures 2b, 3b,d), thus suggesting that, in spite of the no strict stationary conditions of operation, the impedance measurements conform a consistent set of data.

Impedance measurements for samples S1 to S17 and W1 to W3 were essentially coincident with those of reference materials with except of samples S18 and P1 to P11, the Nyquist plots provided two depressed capacitive loops (vide infra).

3.3. Modeling

As previously indicated, for modeling impedance measurements, the coexistence of electrolyte/base electrode and electrolyte/mineral particle interface was initially accounted. For this purpose, equivalent circuits employed to model corroded metal surfaces, modified considering modeling of oxide films with variable degree of coverage and porosity [54,56-58], were used. For modeling the obtained EIS spectra, the simplest equivalent circuit from Lee and Pyun [58] was used. This includes a first resistance (R_s), corresponding to the solution resistance, in series to two parallel branches. The first one contains a parallel association of the charge transfer resistance (R_{ct}) at the graphite/electrolyte interface and the double layer capacitance (C_{dl}). The second branch connects in parallel a constant phase element (Q_p) and a resistance (R_p) associated to the insulating and/or semiconducting particles partially covering the graphite electrode. The fitting to experimental data was significantly improved adding to this second branch an additional resistance (R_i) as schematized in Figure 6a. Figure 7 compares the experimental impedance data for a) cuprite and samples b) S2, c) W2 with the spectra fitted to the equivalent circuit in Figure 6a and the experimental spectrum for sample P11 with the theoretical one by means of fitting to the equivalent circuit in Figure 6b (vide infra). In turn, Figure 8 shows experimental impedance data and the spectrum fitted to the equivalent circuit in Figure 6a for sample S5, in all cases obtaining a satisfactory agreement between theoretical spectra and experimental impedance data.

The above model was satisfactorily fitted to the majority of experimental data (reference compounds and samples S1 to S17 and W1 to W3), as can be seen in Figures 7a-c and 8. The EIS spectra of samples S18 and P1 to P11, although also fitting to the above equivalent circuit, were more satisfactorily fitted to a second, slightly more complex, equivalent circuit depicted in Figure 6b. Here, it was assumed that, as observed in the reduction of lead pigments [59] and glasses [60], metal deposition can also occur via release of metal ions from the ionomeric layer intermediate between the parent solid and the adjacent metal crystals forming a different metallic deposit, so that a new route

(route (v) in Figure S.3) for charge transport can be proposed. The EIS response of this sub-system was modeled in terms of a parallel combination of a resistance (R_{mct}) and a capacitor (C_{mdl}), representative of the charging effects at the metal/electrolyte interface, in Figure 6b. The model in Figure 6b fitted satisfactorily to EIS spectra such as in Figure 7d.

To attribute a physical meaning to the circuit element R_i it is pertinent to consider the peculiar characteristics of the electrochemistry of microparticulate deposits. Since the reduction of cuprite to copper is initiated at the particle/graphite/electrolyte boundary and advances forming an ionomeric layer intercalated between the cuprite and copper phases [52,53], the resistance R_i can be associated to both the ohmic resistance of the ionomeric layer formed as a result of the application of a bias potential promoting the reduction of the copper compound and the charge transfer resistance associated to that process occurring at the three-phase boundary. Table 1 summarizes the values of the different elements of the equivalent circuit in Figure 6a for three experiments involving different amounts of sample S5 transferred onto the graphite electrode.

To rationalize the differences observed between the impedance measurements of different compounds and the amount of mineral transferred onto the electrode surface, one can consider the model from Lee and Pyun [58], previously used to describe the spectra of highly corroded iron [61]. Under the aforementioned conditions of operation, the resistance R_p (Ω) can be associated to the ohmic resistance of the microparticulate deposit of mineral which forms a discontinuous cover on the base graphite so that one can write:

$$R_p = \frac{\delta_p}{\vartheta_p A \sigma_p} \qquad (1)$$

Where δ_p (m), σ_p (Ω^{-1} m^{-1}), are respectively, the thickness of the particle deposit and the conductivity of the material, and ϑ_p the fraction of covered surface area of the graphite electrode, A (m^2). Under our experimental conditions, the discontinuous microparticulate deposit of copper compounds or archaeological materials forms less than a monolayer of crystals over the graphite surface. In these circumstances (see

Scheme in Supplementary materials, Figure S.4), δ_p can be roughly taken as equivalent to the height of the crystals so that, on increasing the amount of solid, there is an increase of the degree of coverage without increasing of the effective thickness of the discontinuous film. Even when the deposit of crystals was more than a monolayer, the surface coverage is higher but only the first line of crystals should contribute effectively to the EIS response which is, as previously noted, dominated by the Faradaic process of reduction of copper compounds to copper metal so that the effective thickness can be reasonably taken as independent on the amount of deposited particles, as schematized in Figure S.4). This view is supported by the fact that the limiting current recorded upon applying a constant potential step of –0.25 V vs. Ag/AgCl was essentially the same regardless the amount of copper compound (see Figure S.1) and that the variation of EIS parameters with the amount of solid sample (see Figures 2b and 3b,d) was moderate.

Due to the insulating and/or semiconducting nature of the copper corrosion products, one can expect that R_p reaches different values for different materials. In turn, the resistance associated to the ionomeric layer formed during the proton-assisted reduction of cuprite to copper metal will produce an ohmic resistance R_{ion} given by:

$$R_{ion} = \frac{\delta_{ion}}{\vartheta_{ion} A \sigma_{ion}} \qquad (2)$$

where δ_{ion} denotes the thickness of the ionomeric layer, σ_{ion} its conductivity, and ϑ_{ion} the fraction of surface area which can be associated to the ionomeric layer. According to modeling introduced to describe the electrochemistry of ion-insertion solids [53], the redox process is initiated at that three-phase junction further expanding through the solid particle via electron transport through the particle/base electrode interface and ion transport through the particle/electrolyte interface. Combining Eqs. (1) and (2), one obtains, eliminating A:

$$R_p = \frac{\delta_p \vartheta_{ion} \sigma_{ion}}{\delta_{ion} \vartheta_p \sigma_p} R_{ion} \qquad (3)$$

On first examination, the resistance of the ionomeric layer, R_{ion}, can be identified as the resistance R_i in the equivalent circuit in Figure 6a. This equation would be independent on the amount of solid particles deposited on the electrode and can be experimentally tested using microparticulate deposits having different surface coverage (and hence different pairs of values of R_{ion} and R_p) and predicts a linear variation of R_p on R_{ion}.

A more detailed examination of the physical situation, however, suggests that R_i should contain an additional term associated to the charge transfer resistance for charge transport through the metal deposit (route (iv) in Figure S.2), R_{ctp}. Taking $R_i = R_{ion} + R_{ctp}$, Eq. (3) yields:

$$R_p = \frac{\delta_p \vartheta_{ion} \sigma_{ion}}{\delta_{ion} \vartheta_p \sigma_p} (R_i - R_{ctp}) \quad (4)$$

Figure 9 depicts the variation of R_p on R_i, calculated from curve fitting, using the equivalent circuit in Figure 6a, for different copper minerals and samples S3 and W3 from impedance measurements in 0.10 M $HClO_4$ of microparticulate deposits having different amounts of solid. Experimental data for cuprite, malachite, brochantite and atacamite in Figure 9 reveal that plots of R_p on R_i can be fitted to straight lines of similar slope and negative ordinate at the origin. This result is in agreement with the theoretical expectance from Eq. (4) assuming that R_{ctp} is different for each corrosion product but essentially independent on its amount. This last feature can be interpreted on considering that, as revealed by AFM-VIMP experiments in Figure 1, under the studied conditions the extent of the formation of metallic copper in the vicinity of the cuprite grains was relatively small and that, as derived from electrolysis experiments such as in Figure S.1 (Supplementary information), the limiting charge passed tends to the same value for each corrosion product regardless the amount of parent copper compound transferred onto the graphite electrode. Accordingly, different corrosion products give rise to different straight lines thus providing a method for testing the composition of solid samples from metal corrosion layers.

In the case of tenorite, however, the variation of R_p on R_i was linear but displaying a positive ordinate at the origin. This feature can be tentatively associated to the fact that the reduction of tenorite takes place at potentials more negative than the applied bias

potential (at which atacamite, brochantite, cuprite and malachite are reduced) [30,32,36], and that this reduction process involves a two-step pathway [62].

In order to test the self consistency of this modeling, it was assumed that the capacitance C_p (F) associated to the CPE Q_p can be expressed as:

$$C_p = \varepsilon_p \frac{A\vartheta_p}{\delta_p} \qquad (5)$$

ε_p being the dielectric permittivity (F m^{-1}) of the particles. Combining Eqs. (1) and (5) one obtains:

$$C_p = \frac{\varepsilon_p}{\sigma_p}\frac{1}{R_p} \qquad (6)$$

This equation predicts a linear relationship between C_p and R_p^{-1} which can be experimentally tested.

In spite of its extreme simplicity, experimental data agreed satisfactorily with the above prediction considering the relation between the Q coefficient of CPEs and effective capacitance, C_p [63]. Figure 10 depicts the plots of Q_p vs. R_p^{-1} from impedance measurements on deposits of atacamite, cuprite, malachite and tenorite in contact with 0.10 M $HClO_4$. In all cases, straight lines passing by the origin, corresponding to the expected proportionality between C_p and R_p^{-1} predicted by Eq. (6), were obtained. One can see in this figure how the cuprite curve differs clearly from the malachite and atacamite curves, but discrimination between them and tenorite is uneasy using the above parameters. Consistently with the results in Figure 9, the data points for the samples S3 and W3 were coincident with the curve for tenorite.

3.4. Sample analysis

In order to compare with previous studies on copper corrosion products [31,32,36], the VIMP response of the archaeological samples was first studied by means of VIMP using aqueous acetate buffer as the electrolyte. Pertinent data are provided as a Supplementary information in Figure S.5. According to their voltammetric response, the

studied samples can be grouped into two main electrochemical types. The first one (type I) is characterized by the presence, in the negative-going potential scan voltammograms (sample W1, Figure S.5a) of a cathodic peak at –0.10 V vs. Ag/AgCl (C_1), attributable to the reduction of copper corrosion products, preceding a shoulder near –0.70 V vs. Ag/AgCl, corresponding to the reduction of dissolved oxygen (C_{ox}). In the positive-going potential scan voltammograms (Figure S.5b), only a broad anodic peak at +0.05 V vs. Ag/AgCl (A_{Cu}) was recorded. This peak corresponds to the oxidative dissolution of the deposit of metallic copper resulting from the electrochemical reduction of copper corrosion products. This voltammetric response was observed for samples S1 to S5 and W1 to W3 with minimal variations.

A second set of samples (type II) displayed cathodic scan voltammograms where the signal C_1 was accompanied by two overlapping tall peaks at –0.57 and –0.72 V vs. Ag/AgCl (conjointly labeled as C_2) superimposed to the C_{ox} background shoulder (Figure S.5c). The group of peaks C_2 can be mainly attributed to the reduction of lead corrosion products, eventually superimposed to the reduction of tenorite (CuO). The presence of lead was unambiguously confirmed by the appearance, in the positive-going scan voltammograms (Figure S.5d) of a sharp anodic peak at –0.55 V vs. Ag/AgCl, (A_{Pb}) corresponding to the stripping oxidative dissolution of metallic lead electrochemically generated as a result of the reduction of lead corrosion products, accompanying the stripping of copper (peak A_{Cu}) at +0.05 V vs. Ag/AgCl. This group included samples S18 and WP1 to WP11. Samples S6 to S17 displayed voltammograms close to that of the type I but showing weak signals C_{Pb} and A_{Pb}.

As previously noted, the EIS response of the studied archaeological samples was closely similar to that of the copper compounds, as can be seen in Figure 9. Examination of impedance data, however, revealed a more complex grouping of the above samples. This can be seen in Figure 11, where the variation of R_p on R_i, calculated from curve fitting using the equivalent circuit in Figure 6a for impedance data for microparticulate deposits having different amounts of solid samples attached to graphite in contact with air-saturated 0.10 M $HClO_4$ solution is depicted. Continuous lines correspond to cuprite, malachite and tenorite (see Figure 9). Data points for samples S1 to S5 (solid squares in Figure 11a) and W1 to W3 (squares in Figure 11b) fall in the region between cuprite

and tenorite lines thus suggesting a common pattern with more or less intense corrosion. Samples S6 to S17, however, fall in a region around a straight line (dotted line in Figures 11a,b) beyond the tenorite line. Taking into account that all samples were extracted from a common archaeological context, the above feature suggested that such samples were constituted by a different metallic substrate. Remarkably, the data points for sample S18 (triangles in Figure 11a) and samples P1 to P11 (solid squares in Figure 11b), all containing relatively high lead amounts, were distributed in a relatively large region of the diagram. Such samples contained relatively large amounts of lead, as denoted by voltammetric data (Figure S.5) so that their location in a region of the diagram clearly separated from that corresponding to the expected copper corrosion products can be attributed to the distorting effect associated to lead. In this regard it is pertinent to note that, in leaded bronzes, lead does not go into solution as in copper but it remains in characteristic globular features more or less regularly distributed into the bronze matrix, thus resulting in the formation of peculiar corrosion patterns [13,14,64,65], including unalloyed copper inclusions [66,67]. This probably results in a situation which cannot be described in terms of the simplified model based on Eqs. (1)-(4) so that the experimental data diverge significantly of the expected behavior. In fact, our previous data on leaded bronze statuary revealed a significant alteration of the VIMP parameters relative to those of bronze [32]. In spite of this, electrochemical impedance measurements can yield sample grouping consistent with VIMP measurements having potential usefulness for studying archaeological samples.

4. Conclusions

Electrochemical impedance measurements on microparticulate deposits of copper corrosion products attached to graphite electrodes in contact with 0.10 M $HClO_4$ aqueous electrolyte provide well-defined frequency responses which depend on the applied bias potential and the amount of solid material transferred onto the base electrode surface. Such impedance measurements can be modeled on the basis of available equivalent circuits for corroded metal surfaces. Under optimized conditions, several pairs of circuit elements provide monotonic variations which are able to characterize different corrosion compounds regardless the amount of microparticulate solid on the electrode.

Application of impedance measurements to a set of archaeological samples from the archaeological Roman site of Gadara (Jordan, 4th century AD) permitted to establish a sample grouping which was entirely consistent with that derived from VIMP measurements, thus illustrating the capabilities of the intersection of such techniques in the archaeometric domain.

Acknowledgements: Financial support from the MINECO Projects CTQ2014-53736-C3-1-P and CTQ2014-53736-C3-2-P which are also supported with ERDF funds and Grants ES-2012-052716 and EEBB-I-16-11558 is gratefully acknowledged.

References

[1] E. Pernicka, Whither metal analysis in archaeology?, in C. Mordant, M. Pernot, and V. Rychner, Eds., L'atelier du bronzier en Europe du XXe au VIIIe siècle avant notre ère, Bronze'96, Tome I, Comité des Travaux Historiques et Scientifiques, Paris (1998) 259–267.

[2] D. Attanasio, G. Bultrini, G.M. Ingo, The possibility of provenancing a series of bronze punic coins found at Tharros (Western Sardinia) using the literature lead isotope database. Archaeometry 43 (2001) 529–547.

[3] D.A. Scott, Copper and bronze in art: corrosion, colorants and conservation, II. Getty Publ. Los Angeles (2002).

[4] I. Constantinides, A. Adriaens, F. Adams, Surface characterization of artificial corrosion layers on copper alloy reference materials. Appl. Surf. Sci. 189 (2002) 90–101.

[5] D.A. Scott, An examination of the patina and corrosion morphology of some Roman bronzes. Journal of the American Institute of Conservation 33 (1994) 1–23.

[6] L. Robbiola, J.M. Blengino, C. Fiaud, Morphology and mechanisms of formation of natural patinas on archaeological CuSn alloys. Corros. Sci. 40 (1998) 2083–2111.

[7] L. Robbiola, R. Portier, A global approach to the authentication of ancient bronzes based on the characterization of the alloy–patina–environment system. J. Cult. Herit. 7 (2006) 1–12.

[8] I. Sandu, C. Marutoiu, I.G. Sandu, A. Alexandru, A.V. Sandu, Authentication of Old Bronze Coins I. Study on Archaeological Patina. Acta Universitatis Cibinensis Section F Chemia 9 (2006) 39–53.

[9] M. Bouchard. D.C. Smith, Catalogue of 45 references Raman spectra of minerals concerning research in art history of archaeology, especially on corroded metal and coloured glass. Spectrochim. Acta A 59 (2003) 2247–2266.

[10] I. De Ryck, A. Adriaens, E. Pantos, F. Adams, A comparison of microbeam techniques for the analysis of corroded ancient bronze objects. Analyst 128 (2003) 1104–119.

[11] L. Selwyn, Metals and corrosion: a handbook for the conservation professional. Ottawa: Canadian Conservation Institute (2004) 122–123.

[12] C. Chiavari, K. Rahmouni, H. Takenouti, S. Joiret, P. Vermaut L. Robbiola, Composition and electrochemical properties of natural patinas of outdoor bronze monuments. Electrochim. Acta 52 (2007) 7760–7769.

[13] J. Cura D'Ars de Figueiredo Junior, V. de Freitas Cunha Lins, V.M. De Bellis, Surface characterization of a corroded bronze-leaded alloy in a salt spray cabinet. Appl.Surf. Sci. 253 (2007) 7104–7107.

[14] M.C. Bernard, S. Joiret, Understanding corrosion of ancient metals for the conservation of cultural heritage. Electrochim. Acta 54 (2009) 5199–5205.

[15] A. Vlasa, S. Varvara, L. Muresan, Electrochemical investigation of the influence of two thiadiazole derivatives on the patina of an archaeological bronze artefact using a carbon paste electrode, Studia Chemia, LII, 2 (2007) 63–73.

[16] F. Scholz, F., B. Meyer, Voltammetry of solid microparticles immobilized on electrode surfaces. Electroanalytical Chemistry, A Series of Advances. Bard, A. J., and Rubinstein, I., Eds., Marcel Dekker, New York 20 (1998) 1–86.

[17] F. Scholz, U. Schröder, R. Gulaboski, A. Doménech-Carbó, Electrochemistry of Immobilized Particles and Droplets. 2nd Edit. Springer, Berlin-Heidelberg (2014).

[18] A. Doménech-Carbó, M. T. Doménech-Carbó, V. Costa, Electrochemical Methods in Archaeometry, Conservation and Restoration. Monographs in Electrochemistry Series, Scholz, F., Ed. Springer, Berlin-Heidelberg (2009).

[19] A. Doménech-Carbó, Voltammetric methods applied to identification, speciation and quantification of analytes from works of art: an overview. J. Solid State Electrochem. 14 (2010) 363–369.

[20] A. Doménech-Carbó, J. Labuda, F. Scholz, Electroanalytical chemistry for the analysis of solids: characterization and classification (IUPAC Technical Report). Pure Appl. Chem. 85 (2013) 609–631.

[21] N. Souissi, L. Bousselmi, S. Khosrof, E. Triki, Voltammetric behaviour of an archeaological bronze alloy in aqueous chloride media. Mater. Corros. 55 (2004) 284–292.

[22] A. Doménech-Carbó, M.T. Doménech-Carbó, I. Martínez-Lázaro, Electrochemical identification of bronze corrosion products in archaeological artefacts. A case study. Microchim. Acta 162 (2008) 351–359.

[23] M. Serghini-Idrissi, M.C. Bernard, F.Z. Harrif, S. Joiret, K. Rahmouni, A. Srhiri, H. Takenouti, V. Vivier, M. Ziani, Electrochemical and spectroscopic characterizations of patinas formed on an archaeological bronze coin. Electrochim. Acta 50 (2005) 4699–4709.

[24] V. Costa, K. Leyssens, A. Adriaens, N. Richard, F. Scholz, Electrochemistry reveals archaeological materials. J. Solid State Electrochem. 14 (2010) 449–451.

[25] D. Satovic, S. Martinez, A. Bobrowski, Electrochemical identification of corrosion products on historical and archaeological bronzes using the voltammetry of micro-particles attached to a carbon paste electrode. Talanta 81 (2010) 1760–1765.

[26] F.A. Gholenji, A. Adriaens, Electrochemical quantification of copper-based alloys using voltammetry of microparticles: optimization of the experimental conditions. J. Solid State Electrochem. 16 (2012) 535–543.

[27] D. Blum, W. Leyffer, R. Holze, Pencil-Leads as New Electrodes for Abrasive Stripping Voltammetry. Electroanalysis 8 (1996) 296–297.

[28] V. Costa, F. Urban, Lead and it alloys: metallurgy, deterioration and conservation, Reviews in Conservation, International Institute of Conservation 6 (2005) 48–62.

[29] A. Doménech-Carbó, M.T. Doménech-Carbó, M.A. Peiró-Ronda, 'One-touch' voltammetry of microparticles for the identification of corrosion products in archaeological lead. Electroanalysis 23 (2011) 1391–1400.

[30] A. Doménech-Carbó, M. Lastras, F. Rodríguez, L. Osete-Cortina, Mapping of Corrosion Products of Highly Altered Archaeological Iron Using Voltammetry of Microparticles. Microchem. J. 106 (2013) 41–50.

[31] A. Doménech-Carbó, M.T. Doménech-Carbó, I. Martínez-Lázaro, Layer-by-layer identification of copper alteration products in metallic works of art using the voltammetry of microparticles approach. Anal. Chim. Acta 610 (2010) 1–9.

[32] A. Doménech-Carbó, M.T. Doménech-Carbó, J. Redondo-Marugán, L. Osete-Cortina, M. V. Vivancos-Ramón, Electrochemical characterization of corrosion products in leaded bronze sculptures considering ohmic drop effects on Tafel analysis. Electroanalysis 28 (2016) 833–845.

[33] A. Doménech-Carbó, M.T. Doménech-Carbó, M.T., Peiró-Ronda, M.A., L. Osete-Cortina, Authentication of archaeological lead artifacts using voltammetry of microparticles: the case of the *Tossal de Sant Miquel* Iberian plate. Archaeometry 53 (2011) 1193–1211.

[34] A. Doménech-Carbó, M.T. Doménech-Carbó, M. Lastras, M. Herrero, M., Detection of archaeological forgeries of Iberian lead plates using nanoelectrochemical techniques, The lot of fake plates from Bugarra (Spain). For. Sci. Int. 247 (2015) 79–88.

[35] A. Doménech-Carbó, M.T. Doménech-Carbó, M.A. Peiró-Ronda, Dating archaeological lead artifacts from measurement of the corrosion content using the voltammetry of microparticles. Anal. Chem. 83 (2011) 5639–5644.

[36] A. Doménech-Carbó, M.T. Doménech-Carbó, S. Capelo, T. Pasíes, I. Martínez-Lázaro, Dating archaeological copper/bronze artifacts using the voltammetry of microparticles. Angew. Chem. Int. Ed. 53 (2014) 9262–9266.

[37] D.D. Macdonald, The history of the point defect model for the passive state: a brief review of film growth aspect. Electrochim. Acta 56 (2011)1761–1772.

[38] F. Sharifi-Asl, M. L. Taylor, Z. Lu, G.L. Engelhardt, B. Kursten, D.D. Macdonald. Modeling of the electrochemical impedance spectroscopic behavior of passive iron using a genetic algorithm approach. Electrochim. Acta 102 (2013) 161–173.

[39] N. Souissi, L. Bousselmi, S. Khosrof, E. Triki, Electrochemical behaviour of an archaeological bronze alloy in various aqueous media: New method for understanding artifacts preservation. Mater. Corros. 54 (2003), 318–325.

[40] N. Souissi, E. Triki, L. Bousselmi, S. Khosrof, Comparaison between archaeological and artificially aged bronze interfaces. Mater. Corros. 57 (2006), 794–799.

[41] N. Souissi, E. Triki, Characterization of ethnographic copper corrosion. Mater. Corros. 60 (2009) 262–268.

[42] A.L. Mata, M.M.L. Salta, M.M.M. Neto, M.H. Mendonça, I.T.E. Fonseca, Characterization of two Roman coins from an archaeological site in Portugal. Mater. Corros. 61 (2010) 205–210.

[43] E. Cano, D. Lafuente, D.M. Bastidas, Use of EIS for the evaluation of the protective properties of coatings for metallic cultural heritage: a review. J. Solid State Electrochem. 14 (2010) 381–391.

[44] A. Doménech-Carbó, M.T. Doménech-Carbó, M.A. Peiró-Ronda, I. Martínez-Lázaro, J. Barrio, Application of the voltammetry of microparticles for dating archaeological lead using polarization curves and electrochemical impedance spectroscopy. J. Solid State Electrochem. 16 (2012) 2349–2356.

[45] A. Doménech-Carbó, S. Capelo, J. Piquero-Cilla, M.T. Doménech-Carbó, J. Barrio, A. Fuentes, W. Al-Sekkaneh. Dating archaeological copper using electrochemical impedance spectroscopy. Comparison with voltammetry of microparticles dating. Mater. Corros. 67 (2016) 120–129.

[46] U. Retter, A. Widmann, K. Siegler, H. Kahlert, On the impedance of potassium nickel(II) hexacyanoferrate(II) composite electrodes–the generalization of the Randles model referring to inhomogeneous electrode materials. J. Electroanal. Chem. 546 (2003) 87–96.

[47] M. Sluyters-Rehbach, J.H. Sluyters, On the meaning of the impedance concept in the case of an object that varies with time and in the case of a swept frequency. J. Electroanal. Chem. 102 (1979) 415–419.

[48] G.S. Popkirov, R.N. Schneider, Validation of experimental data in electrochemical impedance spectroscopy. Electrochim. Acta 38 (1993) 861–867.

[49] D.D. Macdonald, A. Sikora, G. Engelhardt, Characterizing electrochemical systems in the frequency domain. Electrochim. Acta 43 (1998) 87–107.

[50] J.M. Bastidas, J.L. Polo, C.L. Torres, E. Cano, A study on the stability of AISI 316L stainless steel pitting corrosion through its transfer function. Corros. Sci. 43 (2001) 269–281.

[51] A. Doménech-Carbó, M. T. Doménech-Carbó, M. Silva, F.M. Valle-Algarra, J.V. Gimeno-Adelantado, F. Bosch-Reig, R. Mateo-Castro, 2015. Screening and mapping pigments in paintings using scanning electrochemical microscopy (SECM). *Analyst* 140, 1065-1075.

[52] Hasse, U.; Scholz, F. In situ atomic force microscopy of the reduction of lead oxide nanocrystals immobilised on an electrode surface, *Electrochem. Commun.* 2001, 3, 429-434.

[53] U. Schröder, K.B. Oldham, J.C. Myland, P.J. Mahon, F. Scholz, Modelling of solid state voltammetry of immobilized microcrystals assuming an initiation of the electrochemical reaction at a three-phase junction. J. Solid State Electrochem. 4 (2000) 314–324.

[54] G. Chen, C.C. Waraksa, H. Cho, D.D. Macdonald, T.E. Mallouk, EIS Studies of Porous Oxygen Electrodes with Discrete Particles. I. Impedance of Oxide Catalyst Supports. J. Electrochem. Soc. 150 (2003) E423–E428.

[55] M.E. Orazem, N. Pébère, B. Tribollet, J. Electrochem. Soc. 15394 (2006) B129–B136.

[56] G. Nagy, Z. Kerner, R. Schiller, Interpretation of EIS data on passive steel surfaces in aqueous sulfuric acid solution in terms of carrier migration and recombination. Electrochim. Acta 53 (2007) 1737–1742.

[57] J. Zerbino, L. Gassa, Electrochemical impedance spectroscopy study of cuprous oxide films formed on copper: effect of pH and sulfate and carbonate ions. J. Solid State Electrochem. 7 (2003) 177–182.

[58] S.J. Lee, S.L. Pyun, Assessment of corrosion resistance of surface-coated galvanized steel by analysis of the AC impedance spectra measured on the salt-spray-tested specimen. J. Solid State Electrochem. 11 (2007) 829–839.

[59] A. Doménech-Carbó, M.T. Doménech-Carbó, X. Mas-Barberá, Identification of lead pigments in nanosamples from ancient paintings and polychromed sculptures using voltammetry of nanoparticles/atomic force microscopy. Talanta 71 (2007) 1569–1579.

[60] A. Doménech-Carbó, M.A. Villegas, F. Agua, S. Martínez-Ramírez, M.T. Doménech-Carbó, B. Martínez, Electrochemical fingerprint of archaeological lead silicate glasses using the voltammetry of microparticles approach. J. Am. Ceram. Soc. 99, 3915–3923.

[61] A. Doménech-Carbó, M. Lastras, F. Rodríguez, L. Osete-Cortina, Monitoring stabilizing procedures of archaeological iron using electrochemical impedance spectroscopy. J. Solid State Electrochem. 18 (2014) 399–409.

[62] H. Gil, Electrochemical reduction modeling of copper oxides obtained during *in situ* and *ex situ* conditions in the presence of acetic acid. Electrochim. Acta 54 (2009) 4676–4681.

[63] B. Hirschorn, M.E. Orazem, B. Tribollet, V. Vivier, I. Frateur, M. Musiani, Determination of effective capacitance and film thickness from constant-phase-element parameters. Electrochim. Acta 55 (2010) 6218–6227.

[64] N.D. Meeks, Tin-rich surfaces on bronze-some experimental and archaeological considerations. Archaeometry 28 (1986), 133–162.

[65] G.M. Ingo, P. Plescia, E. Engelini, C. Riccucci, T. De Caro, Bronze roman mirrors: The secret of brightness. Appl. Phys. A 83 (2006) 611–615.

[66] Q. Wang, J.F. Merkel, Studies on the redeposition of copper in Jin bronzes form Tianma-Qucun, Shanxi, China. Stud. Conservat. 46 (2001) 242–250.

[67] C. Bosi, L. Garagnani, V. Imbeni, C. Martini, Unalloyed copper inclusions in ancient bronze. J. Mater. Sci. 37 (2002) 4285–4298.

Figures

Figure 1. Three-dimensional topographic images of a microparticulate deposit of cuprite on graphite plate in contact with 0.10 M $HClO_4$, a) before and b) after application of a reductive potential input of –0.25 V vs. Ag/AgCl during 5 min. The arrows indicate the regions where additional grains appear.

Figure 2. Nyquist plots from impedance measurements on: a) an unmodified graphite electrode and three successive impedance runs on the same cuprite-modified graphite electrode and b) three cuprite-modified graphite electrodes containing different mineral loadings, all immersed into air-saturated 0.10 M $HClO_4$ aqueous solutions at pH 1.0. Bias potential of –0.25 V vs. Ag/AgCl.

Figure 3. Variation of a,b) log|*Z*| and c,d) the phase angle on log*f* in impedance measurements on: a,c) an unmodified graphite electrode and three successive impedance runs on the same cuprite-modified graphite electrode and b,d) three cuprite-modified graphite electrodes containing different mineral loadings, all immersed into air-saturated 0.10 M $HClO_4$ aqueous solutions at pH 1.0. Bias potential of –0.25 V vs. Ag/AgCl.

.

Figure 4. Variation with the bias potential of the values of a) $|Z_{low}|$ and b) the maximum phase angle at intermediate frequencies in EIS experiments at unmodified graphite electrodes (squares) and those electrodes modified with cuprite (solid squares) and malachite (triangles) in contact with air-saturated 0.10 M $HClO_4$ at pH 1.0. Mean values of three replicate experiments are represented. The concentration of the electrolyte and the position of the electrodes were unchanged and only the bias potential was varied in the different experiments.

Figure 5. Plots of $-Z_{imag}$ at 0.1 Hz vs. Z_{real} at 0.1 Hz from impedance measurements on graphite electrodes modified with deposits of cuprite (squares), malachite (solid squares), brochantite (triangles) and atacamite (solid triangles) immersed into air-saturated 0.10 M $HClO_4$ aqueous solutions at pH 1.0. Bias potential of –0.25 V vs.

Ag/AgCl. Data for successive runs on the same modified electrode and the 1st run on electrodes containing different mineral loadings are superimposed.

Figure 6. Equivalent circuits used to model EIS spectra of a) reference compounds and samples S1 to S17 and W1 to W3; b) samples S18 and P1 to P11.

Figure 7. Comparison of experimental impedance data (points) with the spectra fitted (continuous lines) to the equivalent circuits in Figure 6 for a) cuprite and samples b) S2, c) W2 and d) P11. Spectra a-c) were fitted to the equivalent circuit in Figure 6a; spectrum d) was fitted to the equivalent circuit in Figure 6b.

Figure 8. Comparison of experimental impedance data (points) with the spectra fitted (continuous lines) to the equivalent circuit in Figure 6a for sample S5. a) Nyquist representation of $-Z_{imag}$ vs. Z_{real} and b) $\log|Z|$ vs. $\log f$ and c) $-\varphi$ vs. $\log f$ plots.

Figure 9. Electrochemical impedance measurements performed on different copper corrosion products and samples S3 and W3 on graphite in contact with air-saturated 0.10 M $HClO_4$ solution at pH 1.0. Variation of R_p on R_i, calculated from curve fitting using the equivalent circuit in Figure 6a, for microparticulate deposits having different amounts of solid. Experimental conditions such as in Figures 2 and 3.

Figure 10. Plots of Q_p vs. R_p^{-1} from electrochemical impedance measurements on deposits of atacamite, cuprite, malachite, tenorite and samples S3 and W3 in contact with 0.10 M $HClO_4$ at pH 1.0. Experimental conditions such as in Figures 2 and 3 after fitting to the equivalent circuit in Figure 6a.

Figure 11. Variation of R_p on R_i, calculated from curve fitting using the equivalent circuits in Figure 6, for microparticulate deposits having different amounts of solid samples attached to graphite in contact with air-saturated 0.10 M $HClO_4$ solution at pH 1.0. Continuous lines correspond to cuprite (c), malachite (m) and tenorite (t). a) solid squares: samples S1 to S5; squares: samples S6 to S17; triangles: sample S18; b) solid squares: samples P1 to P11; squares: samples W1 to W3.

Table(s)

Table 1. Values of the circuit elements used to model EIS spectra of sample S5 from fitting of impedance measurements in conditions such as in Figures 2 and 3 to the equivalent circuit in Figure 6a. Three different amounts of sample were transferred to the base graphite electrode in each measurement. For CPE, $Z_{CPE} = 1/Q(j\omega)^n$. Uncertainties were estimated upon performing three replicate fittings to the same spectrum fixing in ±5 mV the value of R_s obtained in the first unconstrained fitting of this spectrum to the equivalent circuit.

R_s (Ω)	R_{ct} (kΩ)	C_{dl} (F)	R_p (kΩ)	Q_p (Ω $s^{-n)}$)	n	R_i (kΩ)
20±5	3.34±0.02	(2.3±0.2)×10^{-4}	16.4±0.3	(1.8±0.1)×10^{-5}	0.67±0.02	8.90±0.04
25±5	4.79±0.02	(1.8±0.2)×10^{-4}	8.9±0.2	(1.2±0.1)×10^{-4}	0.66±0.02	11.3±0.04
30±5	8.10±0.03	(2.7±0.2)×10^{-4}	7.8±0.2	(2.5±0.1)×10^{-4}	0.66±0.02	12.7±0.04

Figure(s)

Figure 1.

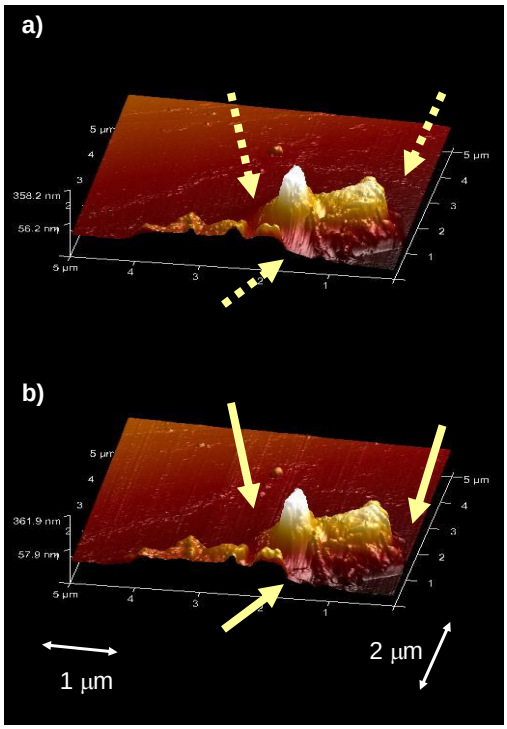

Figure(s)

Figure 2.

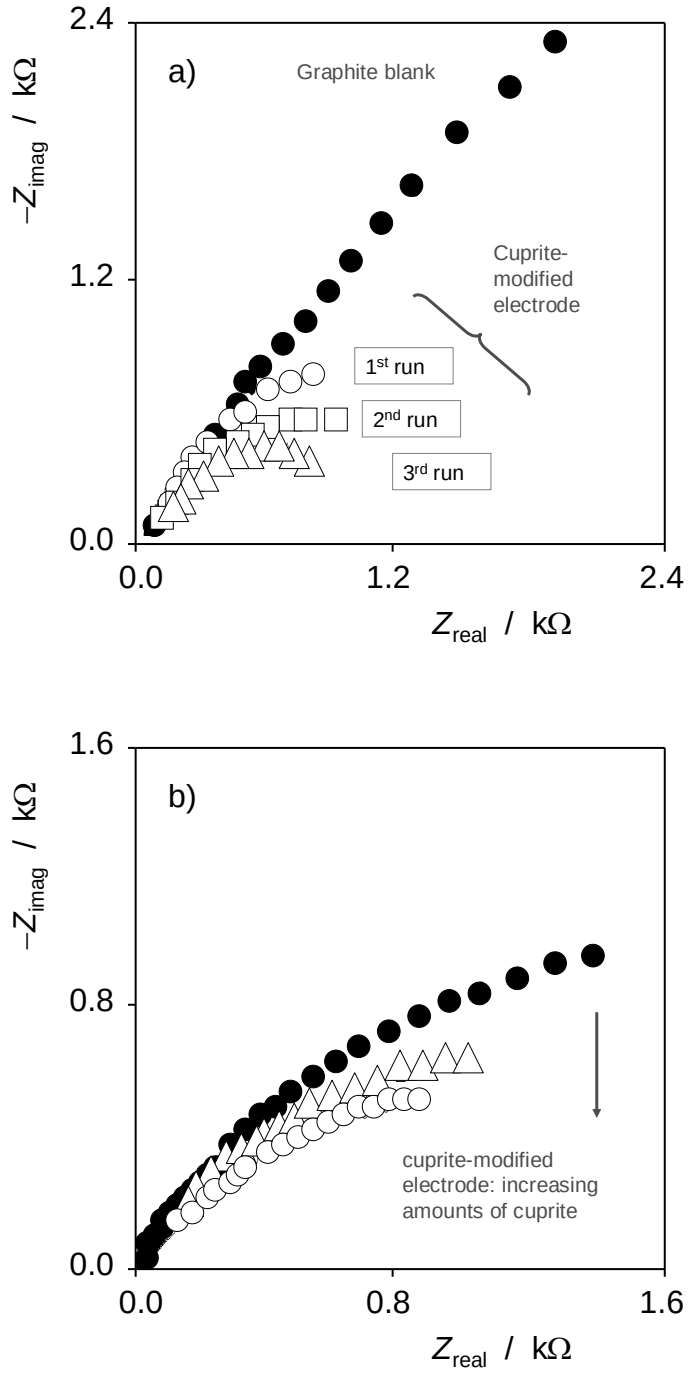

Figure(s)

Figure 3.

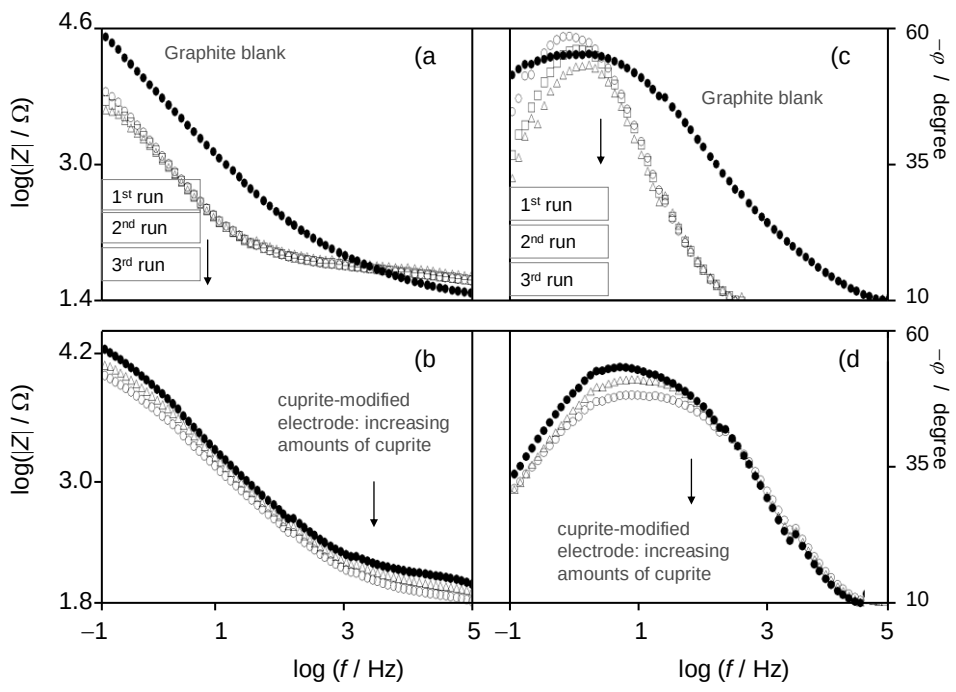

Figure(s)

Figure 4.

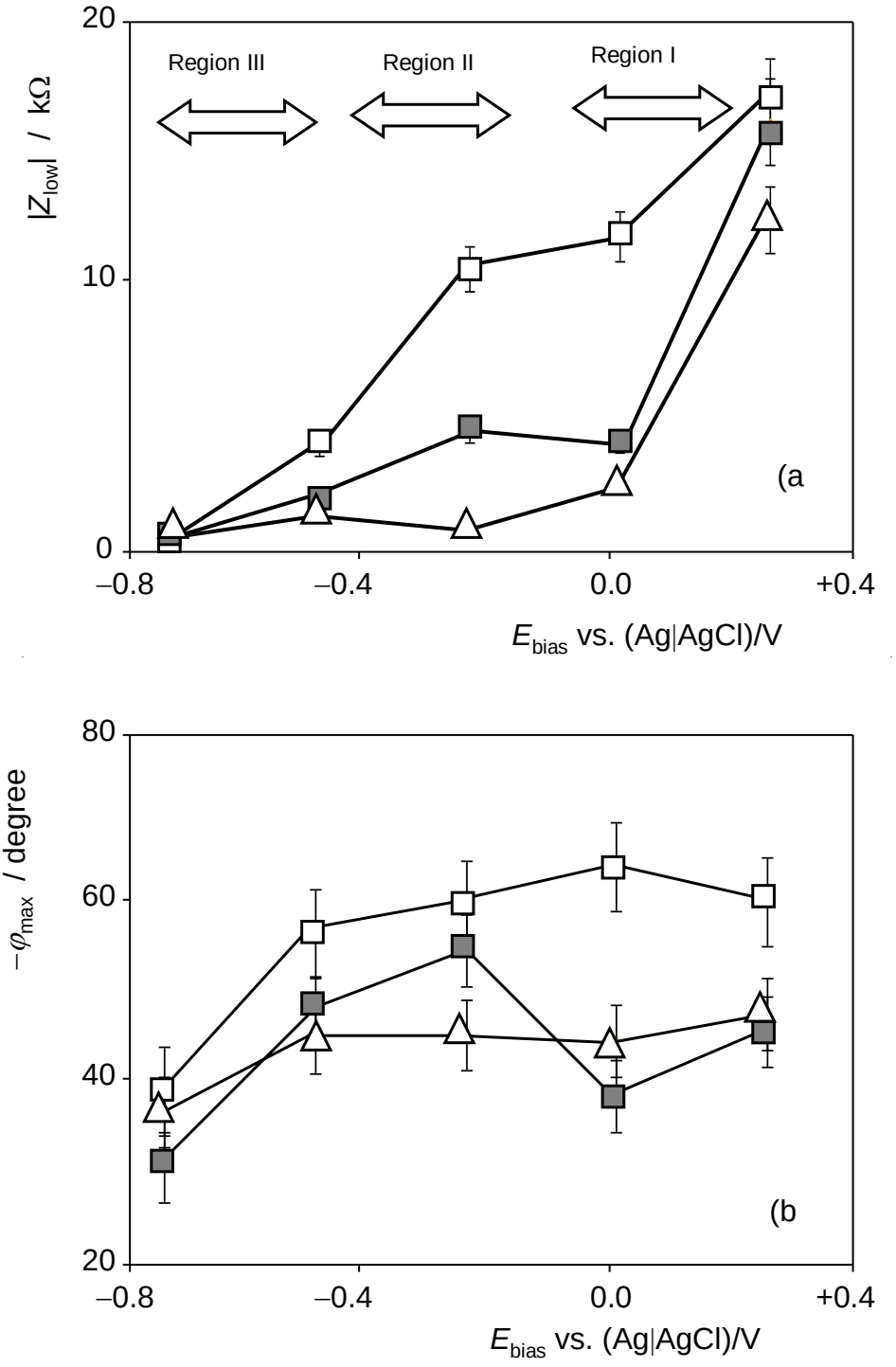

Figure(s)

Figure 5.

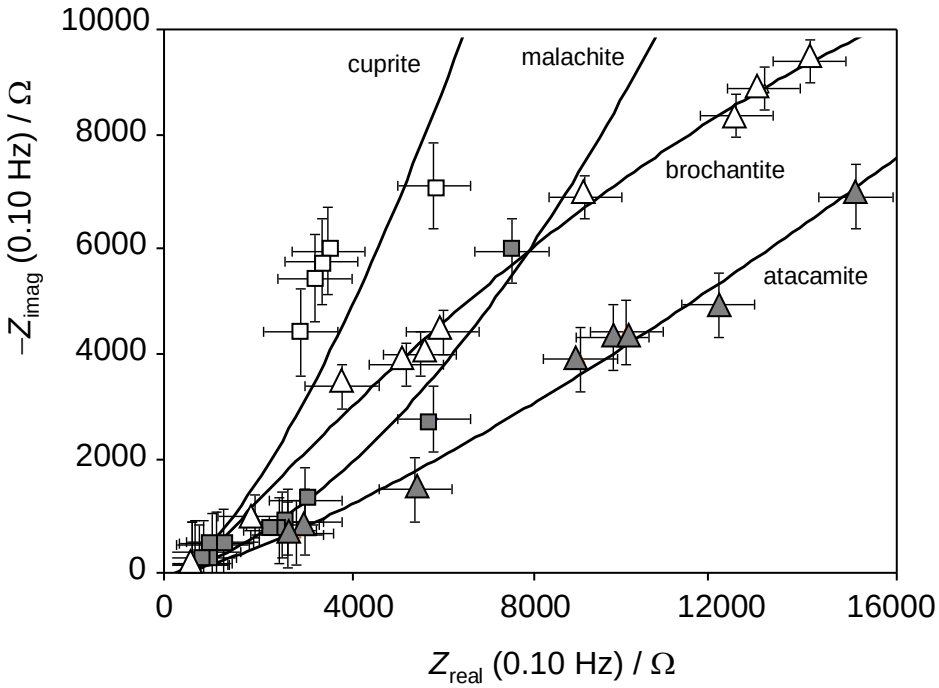

Figure(s)

Figure 6.

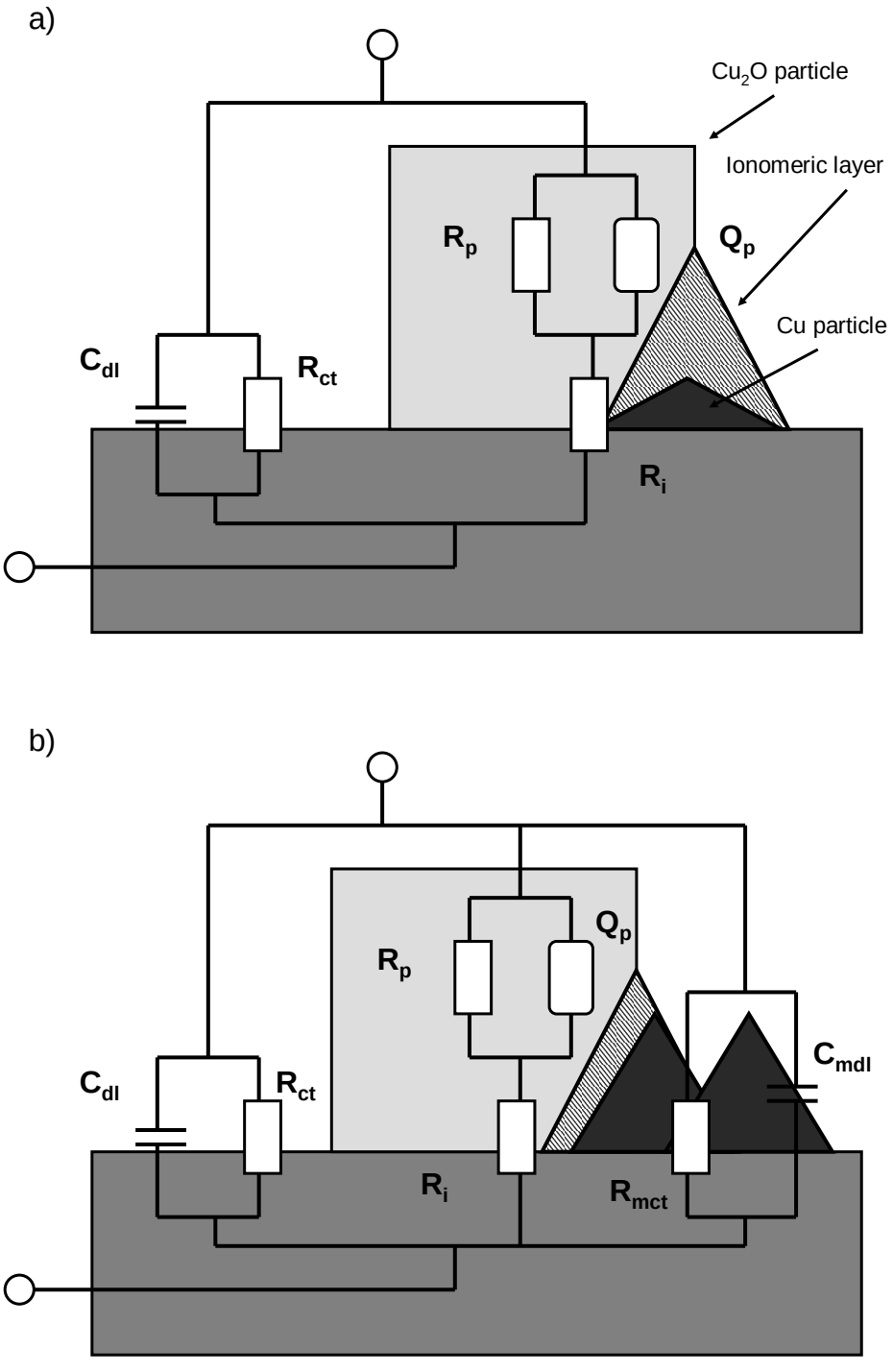

Figure(s)

Figure 7.

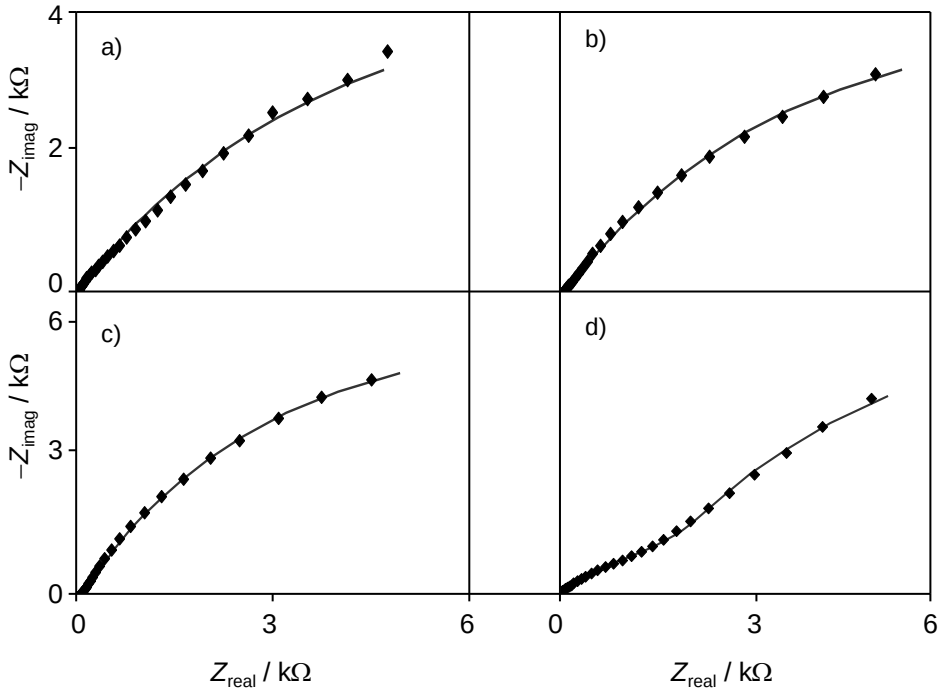

Figure(s)

Figure 8.

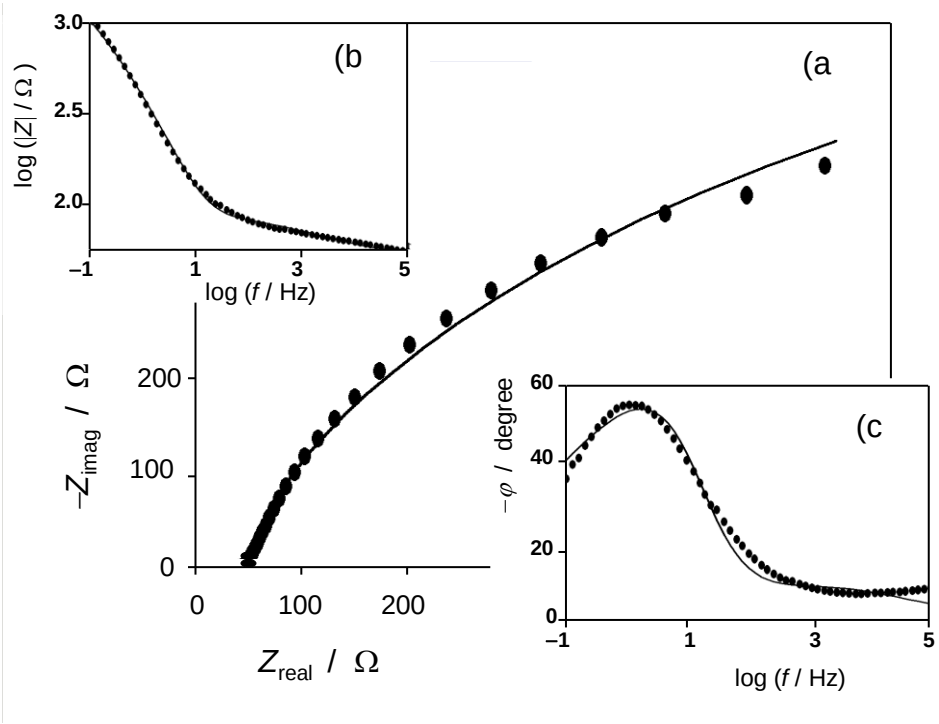

Figure(s)

Figure 9.

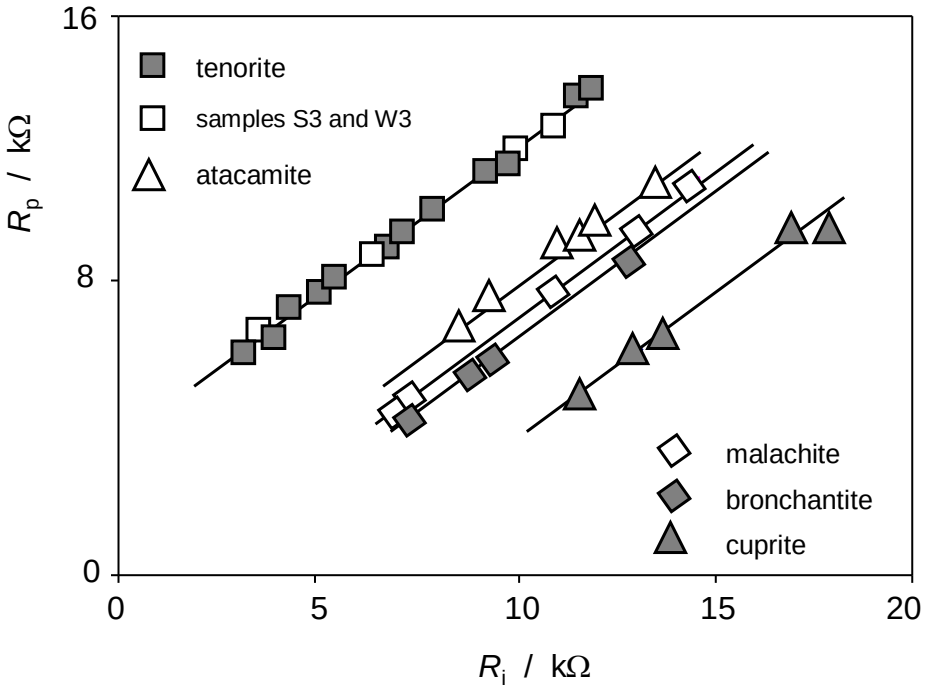

Figure(s)

Figure 10.

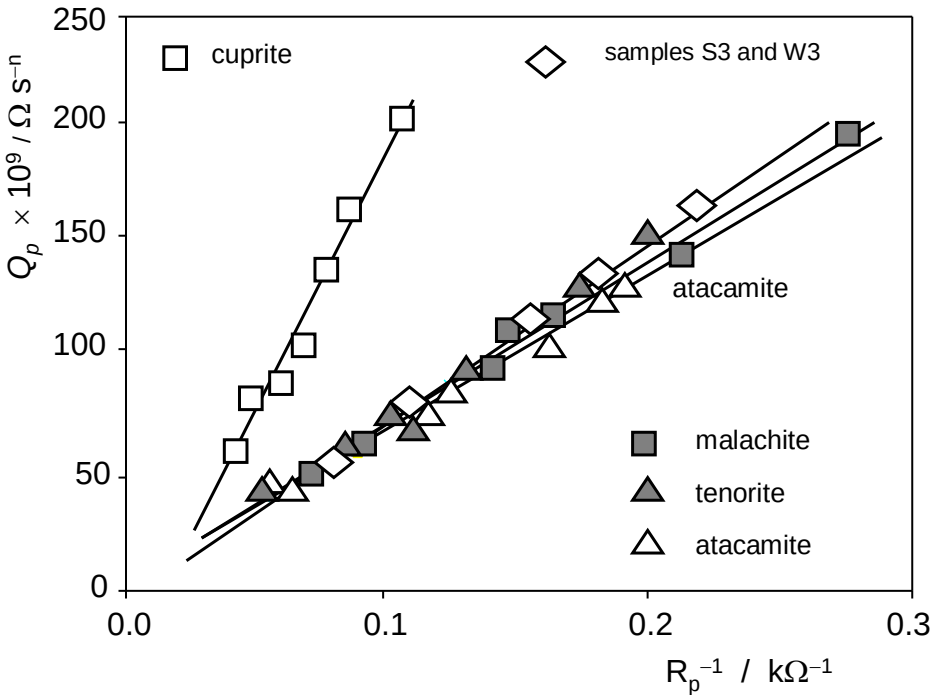

Figure 11.

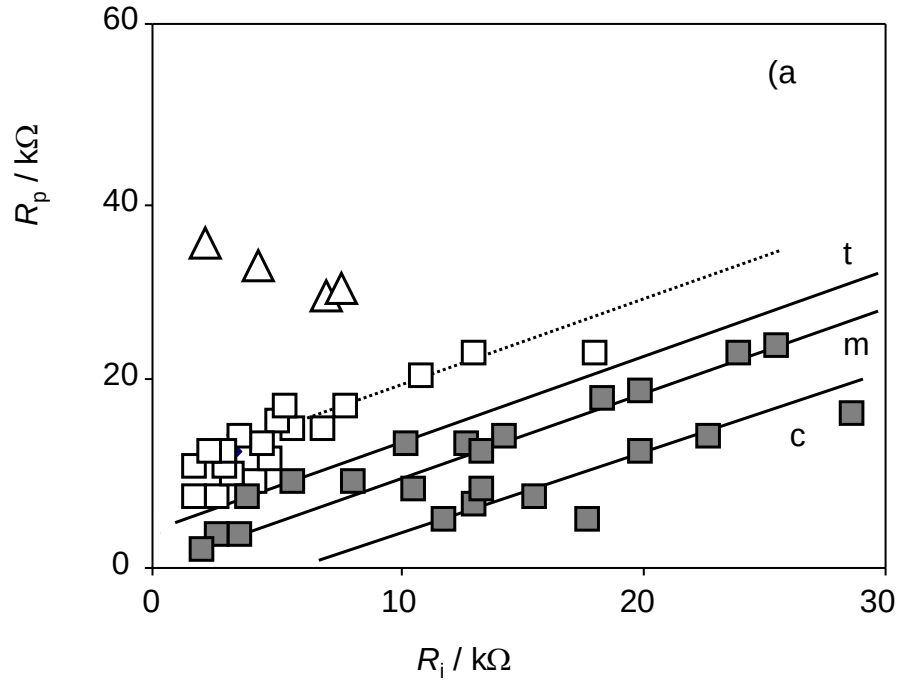
60
40
20
0
0
10
20
30
(a
t
m
c
R_p / kΩ
R_i / kΩ

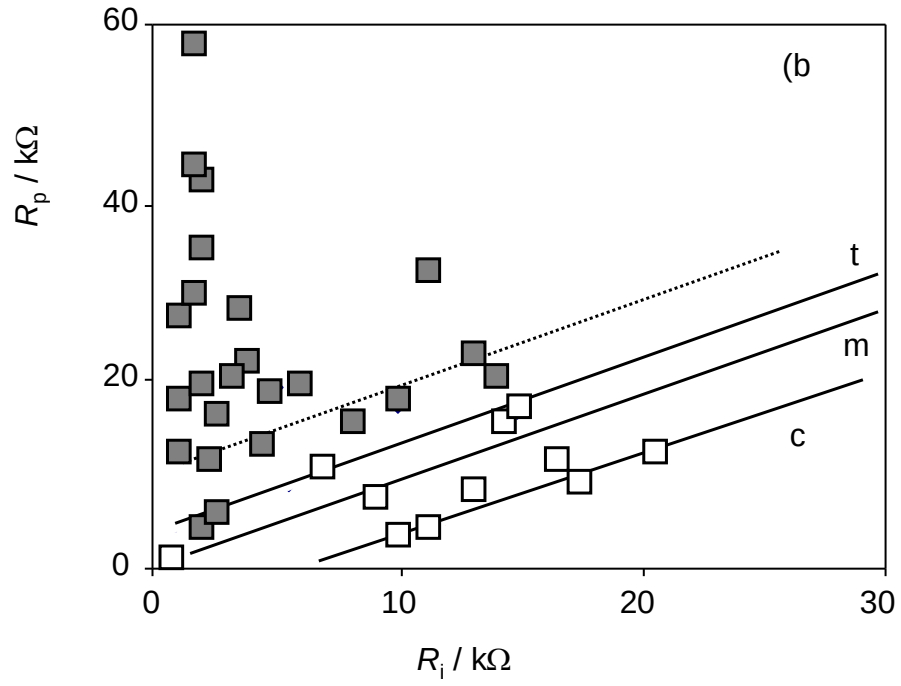
60
40
20
0
0
10
20
30
(b
t
m
c
R_p / kΩ
R_i / kΩ

Supplementary Materials

Click here to download Supplementary Materials: ArticleEISVMPEvora[SupplemMaterRev4].doc